

Variabilities driven by satellite black hole migration in AGN discs

Jing-Tong Xing, Tong Liu^{*}, Bao-Quan Huang, Mouyuan Sun

Department of Astronomy, Xiamen University, Xiamen, Fujian 361005, China

20 January 2025

ABSTRACT

The physical origin of active galactic nucleus (AGN) variability remains unclear. Here we propose that the magnetic reconnection driven by the migration of satellite black holes (sBHs) in the AGN disc can be a new plausible mechanism for AGN short-term variability. During the sBH migration, the co-moving plasmas surrounding the sBH could influence the large-scale magnetic field of the AGN disc and trigger the magnetic reconnections to contribute to AGN UV/optical variability. Meanwhile, the plasma, which is accelerated by the magnetic reconnection, will successfully escape from the disc at Alfvén velocity and cause a secondary magnetic reconnection in the corona. For a $\sim 10^2 - 10^3 M_{\odot}$ sBH (including its binding gas) in the inner regions of the disc surrounding a supermassive black hole with $\sim 10^7 M_{\odot}$, the reconnection process occurred in the space out of the disc can produce X-ray emission, which can last $\sim 10^4 - 10^6$ s with the luminosity $\sim 10^{39} - 10^{43}$ erg s⁻¹.

Key words: accretion, accretion discs - black hole physics - galaxies: nuclei - magnetic reconnection

1 INTRODUCTION

Active galactic nuclei (AGNs) are known to exhibit significant flux variations across multiple wavebands (e.g. McLaughlin, Mullaney, & Littlefair 2024). UV/optical variability is believed to originate from geometrically thick, yet optically thin, accretion discs (e.g. Shakura & Sunyaev 1973), typically displaying small-amplitude, random fluctuations (e.g. Burke et al. 2021). X-ray fluxes also show variability on kilo-second timescales (e.g. Vaughan et al. 2003; McHardy 2013), with the amplitude of variability increasing with the accretion rate and anti-correlating with the mass of the supermassive black hole (SMBH, e.g. Kelly et al. 2013; Lusso & Risaliti 2016). In addition to stochastic variations, AGNs may also exhibit violent flares that significantly deviate from the baseline variability (e.g. Meusinger et al. 2010). However, it remains unclear whether these variations are all driven by a single physical mechanism. Various models have been proposed to explain AGN variability. These include UV/optical variability resulting from variable X-ray reprocessing (e.g. Collin-Souffrin 1991; Krolik et al. 1991), coronal heating and accretion disc reprocessing (e.g. Sun et al. 2020), UV/optical variability driven by global (e.g. Li & Cao 2008; Liu et al. 2016) or local (e.g. Lyubarskii 1997) changes in the accretion rate, and X-ray variability due to coronal flares (e.g. Czerny et al. 2004). Other models include stochastic perturbations in the accretion disc (e.g. Flohic & Eracleous 2008) or X-ray variability arising from a locally unstable, advection-dominated disc (e.g. Manmoto et al. 1996). X-ray variability is generally thought to originate from the hot, optically thin corona in the inner regions of the AGN, which is theoret-

cally linked to magnetohydrodynamic (MHD) instability and turbulence within the corona (e.g. Haardt & Maraschi 1991; Liu, Mineshige, & Shibata 2002).

The accretion disc around an SMBH contains many stars and compact objects that migrate due to density perturbations in the disc gas (e.g. Bellovary et al. 2016). Similar to planetary migration in protoplanetary discs (e.g. Pollack et al. 1996; Armitage 2010), compact objects typically migrate through the AGN disc in one of two modes. When the mass ratio between a compact object and the central SMBH is small enough, such that the compact object migrates rapidly due to disc torque, the migration is referred to as Type I migration. This process has been studied in detail (e.g. Paardekooper et al. 2010; McKernan et al. 2012). If the compact object’s mass is large enough, it can open a gap in the AGN disc (e.g. Syer & Clarke 1995; McKernan et al. 2012). This gap locks the compact object into the viscously driven accretion flow, causing it to migrate more slowly, a process known as Type II migration (e.g. Lin & Papaloizou 1986; Ward 1997; Kanagawa, Tanaka, & Szuszkiewicz 2018).

Planetary migration is accompanied by planetary accretion, which affects the distribution of gas around the planet and its migration rate (e.g. Dürmann & Kley 2017; Li et al. 2021). This effect is also relevant for compact objects. Their interactions with the disc may contribute to X-ray emission, and this contribution should be taken into account when studying AGN variability.

According to MHD simulation results, magnetic reconnection is believed to be common in black hole (BH) accretion discs and coronas, providing energy for jets and AGN flares (e.g. Yuan et al. 2009; Zhang et al. 2018; El Mellah, Cerutti, & Crinquant 2023). Magnetic reconnection generates current sheets due to turbulence

* E-mail: tongliu@xmu.edu.cn

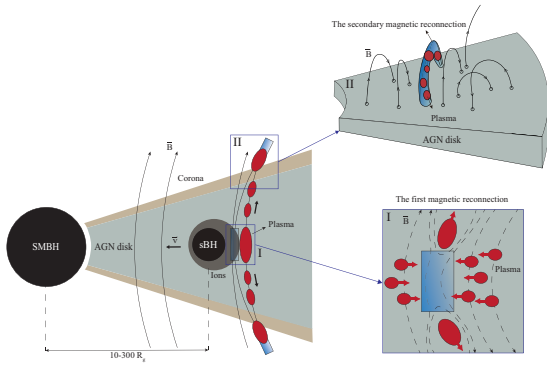


Figure 1. Schematic diagram of the migration model. As an sBH migrates through the AGN disc, its surrounding bound gas becomes ionized into plasma. The ram pressure of the plasma exceeds the magnetic field pressure, altering the magnetic field topology and triggering the first magnetic reconnection (region I) within the disc. This process effectively dissipates magnetic energy and accelerates the plasma. The ejected plasmoid expands and cools within the disc, and highly magnetized plasma can escape at the Alfvén velocity, inducing the second magnetic reconnection (region II) in the AGN corona, which leads to X-ray variability. Additionally, plasma trapped in the disc heats the surrounding gas, contributing to UV/optical variability.

and MHD instability. Under ideal conditions, the magnetic field configuration breaks on the current sheet, creating a plasma chain (or magnetic island) with high magnetization (e.g. Loureiro, Schekochihin, & Cowley 2007; Uzdensky, Loureiro, & Schekochihin 2010). A significant amount of energy from the magnetic field is dissipated through magnetic reconnection, accelerating the resulting plasma (e.g. Komissarov & Barkov 2009; Lyubarsky 2009). The high magnetic field strength in the magnetically arrested disc provides an ideal environment for magnetic reconnection (e.g. Narayan, Igumenshchev, & Abramowicz 2003), a property confirmed in M87 (e.g. Yuan, Wang, & Yang 2022).

In this *Letter*, we investigate a series of magnetic reconnection phenomena triggered by the migration of a satellite black hole (sBH) in the AGN disc. Section 2 discusses the migration speeds under different modes and the conditions that trigger magnetic reconnection during migration. Section 3 presents the numerical analysis results of magnetic reconnection, and the conclusions and discussion are provided in Section 4.

2 MIGRATION

The physical structure of the model is shown in Figure 1. As the surrounding gas bound to the sBH co-migrates inward with the sBH, the co-moving gas becomes ionized, creating ram pressure from the plasma. This pressure affects the magnetic field topology, triggering the first magnetic reconnection and accelerating the plasma. A portion of the plasma that successfully escapes from the disc continues to influence the magnetic field outside the disc, leading to secondary magnetic reconnection in the corona. Meanwhile, the rest of the

plasma clumps trapped in the disc heat the surrounding gas, contributing to the thermal radiation of the AGN disc.

For an SMBH of mass $M_{\bullet} = 10^7 M_{\odot}$ surrounded by a typical AGN disc with the viscous parameter $\alpha = 0.01$ and the dimensionless accretion rate $\dot{m} = \dot{M}/\dot{M}_{\text{Edd}} = 0.15$, where \dot{M} and \dot{M}_{Edd} are the mass accretion rate and Eddington accretion rate, respectively, we consider an sBH (including its accretion gas) of mass M_{sBH} migrating in the AGN disc and assume its initial location is within the AGN disc migration trap ($10 - 300 R_g$, e.g. Bellovary et al. 2016), where $R_g = 2GM_{\bullet}/c^2$ is the Schwarzschild radius of SMBH.

2.1 Migration speeds

Objects embedded in the disc experience different migration patterns with different masses. Generally, migration patterns can be classified into Type I and II migrations. According to the simulations (e.g. Kanagawa, Tanaka, & Szuszkiewicz 2018), for different migration modes, there is a transition condition between two migration types, that is

$$\left(\frac{M_{\text{sBH}}}{M_{\bullet}}\right)_{\text{trans}} = 2.53 \times 10^{-4} \left(\frac{\alpha}{0.01}\right)^{1/2} \left(\frac{h}{0.05}\right)^{5/2}, \quad (1)$$

where the aspect ratio $h = H/R_{\text{sBH}} = 0.05$, and H and R_{sBH} are the disk height and the location of the sBH, respectively. When the ratio of the sBH mass to the SMBH is greater than $(M_{\text{sBH}}/M_{\bullet})_{\text{trans}}$, the migration mode is in Type II; otherwise, it is the Type I migration.

For Type I migration, Paardekooper et al. (2010) proposes that the torque can be described in terms of the linear Lindblad torque and nonlinear horseshoe torque. The Type I migration velocity v_{I} and density ρ_{I} can be simplified to

$$v_{\text{I}} \approx x_s \Omega_{\text{sBH}} = 1.2 \sqrt{\frac{q}{h}} R_{\text{sBH}} \Omega_{\text{sBH}}, \quad (2)$$

and

$$\rho_{\text{I}} = \begin{cases} \rho_0 \left(1 - 2 \frac{\xi}{\tilde{\gamma}} \frac{x}{R_{\text{sBH}}}\right), & 0 < x < x_s, \\ \rho_0, & \text{otherwise,} \end{cases} \quad (3)$$

where $x_s \approx 1.2 \sqrt{q/h} R_{\text{sBH}}$ is the half-width of the horseshoe shaped region (e.g. Paardekooper & Papaloizou 2009), q is the mass ratio of the sBH to the SMBH, $\tilde{\gamma}$ is the adiabatic index, ξ is the initial entropy curve of the power-law index, $\Omega_{\text{sBH}} = (GM_{\bullet}/R_{\text{sBH}}^3)^{1/2}$ is angular velocity of the sBH's orbit, and ρ_0 is the initial density of the AGN disc, respectively.

The classical Type II migration model assumes that the gravitational torque of a massive compact object creates a deep gap in a narrow region, with the density within the gap being low enough for the Type I torque to become inefficient and no flows to cross the gap. Due to the large depth of the gap, the radial flow of gas through it ceases, causing the gas to be blocked and accumulate. The accumulated gas then exerts pressure on the compact object, driving it to move at a viscous speed (e.g. Ivanov, Papaloizou, & Polnarev 1999; Paardekooper et al. 2023). Under these assumptions, the migration velocity and density of sBH were resulted by Equations (40) and (39) in Syer & Clarke (1995).

While other types of migration and more complex torque-induced speed forms may exist, these are generally less stable and can even result in runaway behavior compared to the two types stated here (e.g. Masset & Papaloizou 2003).

2.2 Condition of magnetic reconnection during migration

During migration, when the ram pressure of plasma P_r exceeds the magnetic pressure P_m , the topology of the magnetic field lines can change dramatically, triggering magnetic reconnection. This process is similar to how the solar wind affects the magnetospheric structure of Earth (e.g. Hoyle 1949; Dungey 1961; Hesse & Cassak 2020) and how the “cosmic comb” influences the magnetospheric structure of a pulsar to power fast radio bursts (e.g. Zhang 2017). For a disc with a stable accretion rate, the relation of the magnetic field and accretion rate at R_{sBH} can be expressed as $B = (2\dot{M}c/R_{\text{sBH}}^2)^{1/2}$ (e.g. Ghosh & Abramowicz 1997; Lee, Wijers, & Brown 1999; Liu, Gu, & Zhang 2017). The corresponding magnetic pressure can be calculated as $P_m = B^2/8\pi$.

According to Wald (1974), sBH immersed in a strong magnetic field accumulates an electric charge around it, and this charged sBH generates a magnetic dipole field due to spin (e.g. Dai 2019), which the formation of the magnetic dipole field causes the gas around the sBH to be ionized. In addition, the high temperature of the AGN disc also causes the gas to ionize. The illustration of plasma flow migrating with sBH to form the ram pressure is shown in Figure 1.

For simplicity, we consider that the gas around the sBH has been completely ionizing into a stream of plasmas. The fluid energy-momentum tensor in the lab-frame is $T^{00} = \gamma^2(\rho_c c^2 + e + p) - p = \gamma^2 \rho_c c^2 + (\gamma^2 \hat{\gamma} - \hat{\gamma} + 1)e$, where ρ_c is the co-moving plasmas mass density, e is the initial energy density, $p = (\hat{\gamma} - 1)e$ is the pressure of the fluid, and γ is the Lorentz factor. Subtracting the rest mass energy density, one can obtain the ram pressure of plasmas (e.g. Zhang 2017).

$$P_r = (\gamma^2 - 1)\rho_c c^2 + (\hat{\gamma}\gamma^2 - \hat{\gamma} + 1)e, \quad (4)$$

where

$$\rho_c = \begin{cases} \rho_0(1 - 2\frac{\xi}{\hat{\gamma}}\frac{x_s}{R_{\text{sBH}}}), & M_\odot < M_{\text{sBH}} < 2.5 \times 10^3 M_\odot, \\ \rho_0 \left(\frac{M_D}{M_{\text{sBH}}}\right)^{-\frac{3}{8}}, & \text{otherwise,} \end{cases} \quad (5)$$

and $M_D = 4\pi R_{\text{sBH}}^2 \Sigma_{\text{sBH}}$ is the disc mass with Σ_{sBH} being the surface density at R_{sBH} . Considering a non-relativistic ($\gamma^2 - 1 \approx v/c$) and cold ($e \approx 0$) flow, the ram pressure of plasma can be simplified as $P_r \approx \rho_c v^2$. We assume that the plasma flow and sBH migrate together at the same speed, and the P_r under different migration modes can be expressed as

$$P_r = \begin{cases} \rho_0(1 - 2\frac{\xi}{\hat{\gamma}}\frac{x_s}{R_{\text{sBH}}})v_1^2, & M_\odot < M_{\text{sBH}} < 2.5 \times 10^3 M_\odot, \\ \rho_0 \left(\frac{M_D}{M_{\text{sBH}}}\right)^{\frac{3}{8}} \left(\frac{2}{3}\frac{R_{\text{sBH}}}{\nu_0}\right)^{-2}, & \text{otherwise,} \end{cases} \quad (6)$$

where the viscous drift rate is given by $\nu_0 = \alpha H^2 \Omega_{\text{sBH}}$ (e.g. Shakura & Sunyaev 1973). We consider that $x = x_s$ to calculate the minimum disc density for Type I migration and take the constant $\xi = 1.0$ and $\hat{\gamma} = 5/3$ for the adiabatic disc (e.g. Syer & Clarke 1995).

Based on the above results, we use Sirko & Goodman (2003) proposed an AGN disc model to plot the P_r and P_m during migration. The results are shown in Figure 2, at the migration trap considered in our model (10 – 300 R_g), the

sBH undergoing Type I migration are more prone to trigger magnetic reconnection events in the disc, while massive sBH undergoing Type II migration are less likely to do so. Based on this finding, we only analyze the case of Type I migration in the subsequent calculations.

3 MAGNETIC RECONNECTION

We propose that during sBH migration, two magnetic reconnection events are initiated in the disc and the corona, respectively. We select a set of typical parameter analyses to calculate the process of magnetic reconnection. Considering an sBH with mass $M_{\text{sBH}} = 2 \times 10^2 M_\odot$ (including its accretion gas) migrates in the AGN disc, the speed of migration and the magnetic field strength are

$$v_{\text{I}} = 5.09 \times 10^7 m_{\text{sBH},2}^{1/2} h_{0.05}^{-1/2} r_{\text{sBH},2}^{-1/2} \text{ cm s}^{-1}, \quad (7)$$

and

$$B = 1.20 \times 10^3 \dot{m}_{0.15}^{1/2} r_{\text{sBH},2}^{-1} \text{ G}, \quad (8)$$

respectively, where the dimensionless sBH mass $m_{\text{sBH},2} = M_{\text{sBH}}/(2 \times 10^2 M_\odot)$, $h_{0.05} = h/0.05$, $r_{\text{sBH},2} = R_{\text{sBH}}/(10^2 R_g)$, and $\dot{m}_{0.15} = \dot{M}/(0.15 \dot{M}_{\text{Edd}})$.

3.1 Magnetic reconnection in AGN discs

The sBH with Type I migration may trigger magnetic reconnection due to the tearing instability (e.g. Zenitani & Hoshino 2007), generating current sheets. As shown in the lower right corner of Figure 1, the blue region is referred to as the diffusion region (i.e., current sheet), where magnetic reconnection occurs as the bound plasma streams migrate with the sBH and the magnetic field lines within the AGN disc bend. When two magnetic field lines of opposite directions and the surrounding plasma enter the diffusion region, the topology of the magnetic field changes and the oppositely directed field lines effectively break and reconnect. The reconnected magnetic field lines generate magnetic tension due to strong bending, releasing energy as they straighten, which accelerates plasma heating and forms plasma ejecta (e.g. Hesse & Cassak 2020). Simulations and theoretical studies generally show that the initial structure of the magnetic field breaks within the current sheet, creating plasma chains or magnetic islands (e.g. Loureiro, Schekochihin, & Cowley 2007; Uzdensky, Loureiro, & Schekochihin 2010).

For highly magnetized plasma, the speed approaches the speed of light, and there is a high probability that it can escape the disc. We consider cooling via Coulomb collisions between relativistic electrons and protons to determine whether rapidly cooling plasma cannot escape. The cooling timescale can be estimated as $t_{\text{cool}} \approx \frac{3}{4} \left(\frac{m_e}{2\pi}\right)^{1/2} (\gamma_e m_e c^2)^{3/2} / (e^4 n_p \ln \Lambda)$ (e.g. Spitzer 1962; Cranmer & van Ballegooijen 2012), where e is the electronic charge, m_e is the electronic mass, $n_e = n_p \sim \rho_0/m_p$ is the number density of electrons and protons, and m_p is the proton mass. The Coulomb logarithm is $\ln \Lambda \sim 10$, and γ_e is the Lorentz factor of the electrons in the plasma. When $3.8 \times 10^3 \lesssim \gamma_e \lesssim 3.6 \times 10^4$, the cooling timescale satisfies $t_{\text{cool}} \gtrsim t_{\text{dyn}} \sim H/(\epsilon V_A)$ within 10 – 300 R_g , where t_{dyn} is the dynamic timescales, and $V_A = \sqrt{\sigma/(1 + \sigma)c}$ is the Alfvén velocity. Note that $V_A \sim c$ at high magnetic susceptibility, with $\epsilon \sim 0.1$ being a typical observationally

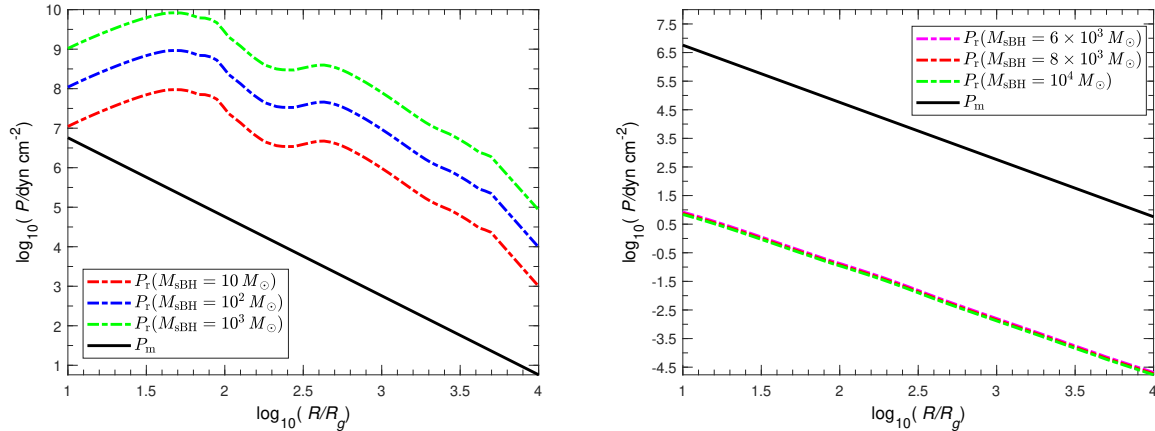


Figure 2. The ram pressure of the plasma and the magnetic pressure in the AGN disc model (Sirko & Goodman 2003) from $10R_g$ to 10^4R_g for $M_\bullet = 10^7M_\odot$, $\dot{m} = \dot{M}/\dot{M}_{\text{Edd}} = 0.15$, and accretion efficiency $\epsilon = 0.1$. The left panel is for the ram pressure of Type I migration for $M_{\text{sBH}} = 10, 10^2$, and $10^3 M_\odot$, and the magnetic pressure; The right panel shows the same result of Type II migration for $M_{\text{sBH}} = 6 \times 10^3, 8 \times 10^3$, and $10^4 M_\odot$.

inferred value (e.g. Giannios 2013). The equipartition argument gives $\gamma_e \sim 3 \times 10^3 \sigma_3$ for the electron in the plasmoid, where $\sigma_3 = \sigma/3$ is the magnetization parameter (e.g. Giannios 2013). This means that the magnetization parameter of the plasma escaping the disc needs to be satisfied $\sigma \geq 3.8$.

The simulation results by Nathanail et al. (2020) show that the plasma may be excited when the magnetization parameter $\sigma \geq 3$ (also see e.g. Li et al. 2017; Bower et al. 2018). This result is consistent with the magnetization parameters required by the cooling timescales and the dynamic timescales. However, this is not always the case, and parts of the plasma will be advected and accreted by the sBH, or bound to the disc. These plasmas contain a large number of relativistic particles, which may be the origin of flares on the AGN disc (e.g. Giannios 2013; Li et al. 2017). Since these plasma spheres are generally thought to be filled with high-energy particles, the parts of the AGN disc that do not break through may contribute to the disc’s thermal radiation. If we consider sBHs uniformly distributed in a two-dimensional plane $N(R)$, and the luminosity released L_{th} by magnetic reconnection is converted into the thermal energy of the disc, then the heating rate can be given as $L_{\text{sBH}}^+ = N(R)L_{\text{th}}$. The distribution of sBHs, i.e., (e.g. Zhou et al. 2024)

$$N(R) = \frac{2R_{\text{sBH}}\Delta RN_{\text{sBH}}}{(R_{\text{out}}^2 - R_{\text{in}}^2)}, \quad (9)$$

where N_{sBH} is the total number of sBHs. For the plasma whose cooling time is less than the dynamic time, its kinetic energy will be converted into heat energy in the disc, thereby heating the gas. We assume that $N_{\text{sBH}} = 10^3$ in a region ($R_{\text{out}} = 300 R_g$, $R_{\text{in}} = 10 R_g$) and consider all the magnetic field energy during $t_{\text{cool}} \sim t_{\text{dyn}}$ was given to the thermal radiation. Otherwise, we expect that the migration velocity affects the volume range of magnetic energy that sBH can control during t_{dyn} , and the faster the migration, the more magnetic field energy can be released simultaneously. Thus, for Kepler’s rotating disc, the entire volume of the magnetic reconnection region in the disc is $V \sim (\Omega_{\text{sBH}}t_{\text{dyn}}R_{\text{sBH}})H(v_{\text{I}}t_{\text{dyn}})$ since $\Omega_{\text{sBH}}t_{\text{dyn}} < 2\pi$ (e.g.

Wang et al. 2018; Dai 2019), then the thermal luminosity is

$$L_{\text{th}} \approx \frac{B^2V}{8\pi t_{\text{dyn}}} = \frac{B^2(\Omega_{\text{sBH}}t_{\text{dyn}}R_{\text{sBH}})Hv_{\text{I}}}{8\pi} \quad (10)$$

$$= 9.02 \times 10^{38} m_{\bullet,7}^{1/2} m_{\text{sBH},2}^{1/2} \dot{m}_{0.15} h_{0.05}^{-1/2} r_{\text{sBH},2}^{-1} \text{ erg s}^{-1},$$

can get $L_{\text{sBH}}^+/(Q_{\text{vis}}^+ 2\pi R_{\text{sBH}}\Delta R) \gtrsim 1.00$ when $R_{\text{sBH}} > 210R_g$ is satisfied, where $m_{\bullet,7} = M_\bullet/(10^7 M_\odot)$ is the dimensionless SMBH mass, Q_{vis}^+ represent the disc viscous heat production, i.e., $Q_{\text{vis}}^+ = (3GM_\bullet\dot{M}f_r)/(8\pi R_{\text{sBH}}^3)$ and $f_r = 1 - (3R_g/R_{\text{sBH}})^{1/2}$. Assuming that sBHs are bound to a certain radius on the AGN disc due to migration traps, the migration of sBHs may affect the effective temperature at that radius, thus dominating the AGN UV/optical variability.

3.2 Magnetic reconnection in AGN coronas

The accelerated plasma carries a large number of relativistic particles, which will greatly enhance the magnetic turbulence in the AGN corona, resulting in secondary magnetic reconnection. However, the magnetic field in the accretion disc is usually turbulent, and the plasma does not escape strictly perpendicular to the disc, but is likely to be trapped inside the disc. The situation described here is more likely to occur in the AGN disc with low luminosity and high magnetic field when the plasma escapes the AGN disc along the magnetic field lines.

The AGN corona is thought to be similar to the solar corona in that it contains hot, quasi-spherical plasma, which contributes to the power-law component of the X-ray spectrum of the accreting black hole (e.g. Bisnovaty-Kogan & Blinnikov 1976; Liang & Price 1977). Due to the interchange instability, the magnetic field is buoyant and rises into the corona, where it dominates the magnetic structure (e.g. Galeev, Rosner, & Vaiana 1979; Tout & Pringle 1992). We propose that most of the magnetic field in the AGN corona exists in the form of magnetic rings or flux ropes (e.g. Uzdensky & Goodman 2008). These rings represent closed magnetic fields (as shown in the upper right corner of Figure 1, where the foot points of the rings are anchored

at different radii on the disc surface). Magnetic rings floating on the disc surface can be twisted and stretched by differential Kepler rotation and turbulence in the accretion flow, causing the rings to expand (e.g. [Uzdensky & Goodman 2008](#)). During torsion and expansion, the rings may undergo internal destruction due to MHD instabilities, or they may reconnect with other rings, releasing magnetic energy stored in the AGN corona (e.g. [Hirose et al. 2004](#); [Goodman & Uzdensky 2008](#); [Yuan et al. 2009](#)).

We hypothesize that the AGN coronal environment initially maintains a force-free condition with a strong magnetic field. However, with the injection of plasma jets from the disc, the magnetic environment becomes perturbed, causing the closed magnetic loops in the corona to intertwine and triggering magnetic reconnection.

We propose that the turbulent motion of the surface magnetic foot may be amplified by the influence of the plasma jet, leading to the evolution of current sheets of various scales in the corona (e.g. [Parker 1972, 1983](#)) and subsequent magnetic reconnection within them. For the magnetic field in the corona, we consider that the initial conditions must satisfy certain permeability criteria to maintain the force-free state. If the initial state of the corona is stable, i.e., the average Lorentz factor of positrons is $\bar{\gamma} = 1$, then the maximum initial plasma density in the corona is (e.g. [El Mellah et al. 2022](#); [El Mellah, Cerutti, & Crinquand 2023](#))

$$n_{0,\max} = \frac{B^2}{4\pi m_e c^2 \bar{\gamma} \sigma} = 1.39 \times 10^{11} \sigma_0^{-1} \dot{m}_{0.15} r_{\text{sBH},2}^{-2} \text{ cm}^{-3}, \quad (11)$$

where $\sigma_0 = \sigma/10^0$. To maintain the initial powerlessness approximation condition, the initial plasma density $n_0 = (n_{0+} + n_{0-}) > n_{\text{GJ}}$ must be satisfied (e.g. [El Mellah, Cerutti, & Crinquand 2023](#)), where n_{GJ} is the Goldreich-Julian charge density. And we can calculate the Goldreich-Julian charge number density by ([Goldreich & Julian 1969](#))

$$n_{\text{GJ}} = -\frac{\mathbf{\Omega} \cdot \mathbf{B}}{2\pi c e} = 9.47 \times 10^{-5} m_{\bullet,7}^{1/2} \dot{m}_{0.15}^{1/2} r_{\text{sBH},2}^{-5/2} \text{ cm}^{-3} \ll n_{0,\max}, \quad (12)$$

where $\mathbf{\Omega}$ is the angular velocity vector of the magnetic field line. Hence, Equation (12) suggests that the magnetic field on the corona is initially held in a force-free state. This result shows that the radial foot separation of the coronal flux loop changes only relatively slowly depending on Kepler-differential rotation alone and that the underlying disc turbulence can greatly affect the random walk of the magnetic foot (e.g. [Uzdensky & Goodman 2008](#)).

Suppose the injection of plasma clumps is considered. In that case, both the plasma density in the corona and the Lorentz factor of the particles change, thus intensifying the magnetic turbulence in the corona. Due to the gas around sBH being ionized, we assume that the initial density of the gas in the disc is equal to the density of the plasma thrown, the number density of the injected plasma mass can be estimated as

$$n_{\text{int}} \approx \frac{\rho_c}{m_p} \sim \frac{\rho_0}{m_p} = 5.99 \times 10^{15} \rho_{-8} \text{ cm}^{-3} \gg n_{0,\max}, \quad (13)$$

where $\rho_{-8} = \rho_0/(10^{-8} \text{ g cm}^{-3})$. When the force-free state in the corona is destroyed, the magnetic field lines outside the disc will also change due to the change in the plasma distri-

bution of the corona (e.g. [Yuan et al. 2009](#); [Nathanail et al. 2020](#); [El Mellah, Cerutti, & Crinquand 2023](#)).

Considering that the density of the gas and the density of the ionized electrons are related, it is then natural to think that the magnetic reconnection caused by the migration may no longer be active near the inner disc regions because the gas density is low. The results in Figure 2 also show a downward trend of ram pressure in the inner region of the disc. To estimate the shortest migration timescale for the sBH position R_{sBH} , we consider the inner regions ($R_{\text{mig}} \sim 20 R_g$) where magnetic reconnection due to migration no longer dominates the emission of radiation. Notably, there are still certain mechanisms capable of triggering magnetic reconnection in the disc, such as MHD instability (e.g. [Nathanail et al. 2020](#)) or magnetospheric collisions resulting from rotation (e.g. [El Mellah et al. 2022](#)). Still, these mechanisms need to be triggered in the vicinity of SMBH. The migration time at $R_{\text{sBH}} = 100 R_g$ can be estimated by

$$t_m = \frac{R_m}{v_I} = \frac{R_{\text{sBH}} - R_{\text{mig}}}{v_I} \approx 4.66 \times 10^6 m_{\text{sBH},2}^{-1/2} h_{0.05}^{1/2} r_{\text{sBH},2}^{1/2} r_{m,80} \text{ s}, \quad (14)$$

where $r_{m,80} = R_m/(80 R_g)$ is migration distance. In fact, the migration timescale should be $\gg t_m$ at R_{sBH} (e.g. [McKernan et al. 2012](#)), here we just give a lower bound. The characteristic duration of the magnetic reconnection is usually described by the global reconnection timescale $t_r \sim l/\epsilon V_A$. The scale height of the magnetic field in the corona should be comparable to the corona height. Based on the restriction of AGN corona height by [Alston et al. \(2020\)](#), we consider the height of the magnetic reconnection out of the disc to be $H_r \sim 15 R_g$. When the line of sight is perpendicular to the disc (this is to maximize the observation and should actually be multiplied by an angle coefficient of less than one), the characteristic scale along the line of sight is $l \sim H_r$. Hence, the duration of the magnetic reconnection is

$$t_r = \frac{l}{\epsilon V_A} \approx 1.48 \times 10^4 l_{15} \text{ s}, \quad (15)$$

where $l_{15} = l/(15 R_g)$. It can be seen that the migration time $t_m \gg t_r$, which indicates that the sBH is likely to cause catastrophic magnetic reconnection during the migration process, resulting in continuous, longer-lasting flares.

The total magnetic energy can be calculated as $B^2 V/8\pi$. As the same as Equation (10), the magnetic reconnection luminosity of the corona is

$$L_r \approx \frac{B^2 V}{8\pi t_r} = 4.06 \times 10^{39} m_{\bullet,7}^{1/2} m_{\text{sBH},2}^{1/2} \dot{m}_{0.15} h_{0.05}^{-1/2} r_{\text{sBH},2}^{-3} h_{r,15} l_{15} \text{ erg s}^{-1}, \quad (16)$$

where $h_{r,15} = H_r/(15 R_g)$ is height of the magnetic reconnection and $r_2 = R_{\text{sBH}}/(100 R_g)$. As can be seen from Equation (16), the luminosity increases with the mass of sBH and decreases with the radius. Powerful magnetic reconnection may be triggered within less than $20 R_g$ as shown in Figure 2. If we consider that there is an intermediate-mass BH in the disc region undergoing Type I migration, the luminosity released during the migration is $\sim 1.44 \times 10^{43} \text{ erg s}^{-1}$ for $M_{\text{sBH}} = 2.5 \times 10^3 M_\odot$ and $R_{\text{sBH}} = 10 R_g$. This luminosity can be comparable with the AGN X-ray luminosity. Based

on the $L_{2\text{keV}} - L_{2500}$ relation ($\log L_{2\text{keV}} = \omega \log L_{2500} + \beta$) with a slope ω of $\sim 0.6-0.65$ and intercept β of $\sim 7-8$ (e.g. [Lusso & Risaliti 2016](#)), we can estimate the AGN X-ray luminosity of $\sim 10^{43} \text{ erg s}^{-1}$ for an accretion rate of $\sim 0.15 \dot{M}_{\text{Edd}}$ by assuming that L_{2500} is consistent with the Eddington luminosity. Hence, our work presents a new mechanism to account for rapid (hours) X-ray variability in AGNs.

Assuming the power of corona is $P_{\text{corona}} = \eta L_{\text{Edd}}$, where $\eta \sim 0.1$ is the coronal power as a proportion of Eddington's luminosity L_{Edd} , we can estimate the ratio of magnetic reconnection dissipation rate to power, i.e. $L_{\text{max}}/P_{\text{corona}} \approx 0.76$. This means that in our model, magnetic reconnection is the main dissipative mechanism in the AGN corona, and other radiation may be a function of turbulence and viscous dissipation.

4 CONCLUSIONS AND DISCUSSION

In this *Letter*, we have investigated the AGN variability caused by the sBH migration. For objects migrating in the AGN disc that are subjected to torques caused by perturbations in disc density, [Bellovary et al. \(2016\)](#) shows that migrating objects in different directions will meet due to changes in the sign of the torques, forming a migration trap. In the migration trap, massive sBHs can be formed efficiently. In this study, we have analyzed the magnetic reconnection triggered by the sBH during different types of migration. The main conclusions are as follows:

(i) We demonstrate that the co-moving plasmas surrounding the sBH are more likely to influence the large-scale magnetic field during Type I migration. This interaction drives the initial magnetic reconnection within the AGN disc.

(ii) For the first magnetic reconnection, we analytically estimate the thermal luminosity released due to plasma cooling as $L_{\text{th}} \sim 9.02 \times 10^{38} \text{ erg s}^{-1}$ for the reconnection occurred at $R_{\text{sBH}} = 100 R_{\text{g}}$. If we consider the presence of 10^3 sBH in the region between $10 R_{\text{g}}$ and $300 R_{\text{g}}$, the thermal radiation resulting from migration can influence the effective temperature of the disc, contributing to UV/optical variability.

(iii) For the second magnetic reconnection, our results show that for a $\sim 10^2 - 10^3 M_{\odot}$ sBH (including its binding gas) in the inner regions of the disc surrounding an SMBH with $\sim 10^7 M_{\odot}$, the reconnection process occurs in the space out of the disc can produce X-ray emission, which can last $\sim 10^4 - 10^6$ s with the luminosity $\sim 10^{39} - 10^{43} \text{ erg s}^{-1}$.

The total magnetic field energy accumulated by the migration of sBH in the reconnection time t_{r} can be estimated as $E_{\text{m}} \sim (B^2 \Omega_{\text{sBH}} R_{\text{sBH}} v_{\text{tr}}^2) (H_{\text{r}} + H) / (8\pi)$, which is derived from the kinetic energy $E_{\text{k}} \sim 10^{50} \text{ erg}$ of sBH according to the conservation of energy. The efficiency of the first magnetic reconnection occurred at $R_{\text{sBH}} = 100 R_{\text{g}}$ can be calculated as $L_{\text{th}} t_{\text{dyn}} / E_{\text{m}} \sim 0.055$. Similarly, the efficiency of the second magnetic reconnection at $R_{\text{sBH}} = 100 R_{\text{g}}$ is given by $L_{\text{r}} t_{\text{rec}} / E_{\text{m}} \sim H_{\text{r}} / (H_{\text{r}} + H) \approx 0.75$. This result indicates that nearly 80% of the magnetic energy released during the magnetic reconnection process is converted into radiation, including $\sim 5\%$ of it emitted as thermal radiation and $\sim 75\%$ released as X-ray radiation.

It should be noted that the gas density formula we use here is independent of the accretion rate, and future modifications

to this formula will be necessary. Additionally, considering that other compact objects, such as white dwarfs and neutron stars, also migrate in AGN discs, the migration of a single low-mass compact object is unlikely to significantly affect the large-scale magnetic field structure of the AGN disc. It has been suggested that massive nuclear cluster objects (NCOs), which consist of stars and compact objects, surround SMBHs and migrate and merge within the disc (e.g. [McKernan et al. 2012](#)). We believe that binary accretion systems within these NCOs could produce effects similar to those arising from the migration of massive sBHs.

ACKNOWLEDGMENTS

We thank Yun-Feng Wei, Shuying Zhou, Jiao-Zhen She, and Xiao-Yan Li for the helpful discussion. This work was supported by the National Key R&D Program of China under grants 2023YFA1607902 and 2023YFA1607903, the National Natural Science Foundation of China under grants 12173031, 12494572, 12221003, and 12322303, the Natural Science Foundation of Fujian Province of China (No. 2022J06002), the Fundamental Research Funds for the Central Universities (No. 20720240152), and the China Postdoctoral Science Foundation under grant 2024M751769.

DATA AVAILABILITY

The data underlying this article will be shared on reasonable request to the first author.

REFERENCES

- Alston W. N., Fabian A. C., Kara E., Parker M. L., Dovciak M., Pinto C., Jiang J., et al., 2020, *NatAs*, 4, 597. doi:10.1038/s41550-019-1002-x
- Armitage P. J., 2010, *apf.book*
- Bellovary J. M., Mac Low M.-M., McKernan B., Ford K. E. S., 2016, *ApJL*, 819, L17. doi:10.3847/2041-8205/819/2/L17
- Bisnovatyi-Kogan G. S., Blinnikov S. I., 1976, *SvAL*, 2, 191. doi:10.48550/arXiv.astro-ph/0003275
- Bower G. C., Broderick A., Dexter J., Doleman S., Falcke H., Fish V., Johnson M. D., et al., 2018, *ApJ*, 868, 101. doi:10.3847/1538-4357/aae983
- Burke C. J., Shen Y., Blaes O., Gammie C. F., Horne K., Jiang Y.-F., Liu X., et al., 2021, *Sci*, 373, 789. doi:10.1126/science.abg9933
- Clarke C. J., Lin D. N. C., Pringle J. E., 1990, *MNRAS*, 242, 439. doi:10.1093/mnras/242.3.439
- Collin-Souffrin S., 1991, *A&A*, 249, 344
- Cranmer S. R., van Ballegoijen A. A., 2012, *ApJ*, 754, 92. doi:10.1088/0004-637X/754/2/92
- Czerny B., Róžańska A., Dovciak M., Karas V., Dumont A.-M., 2004, *A&A*, 420, 1. doi:10.1051/0004-6361:20035741
- Dai Z. G., 2019, *ApJL*, 873, L13. doi:10.3847/2041-8213/ab0b45
- Duney J. W., 1961, *PhRvL*, 6, 47. doi:10.1103/PhysRevLett.6.47
- Dürmann C., Kley W., 2017, *A&A*, 598, A80. doi:10.1051/0004-6361/201629074
- El Mellah I., Cerutti B., Crinquand B., Parfrey K., 2022, *A&A*, 663, A169. doi:10.1051/0004-6361/202142847
- El Mellah I., Cerutti B., Crinquand B., 2023, *A&A*, 677, A67. doi:10.1051/0004-6361/202346781

- Flohic H. M. L. G., Eracleous M., 2008, *ApJ*, 686, 138. doi:10.1086/590547
- Galeev A. A., Rosner R., Vaiana G. S., 1979, *ApJ*, 229, 318. doi:10.1086/156957
- Ghosh P., Abramowicz M. A., 1997, *MNRAS*, 292, 887. doi:10.1093/mnras/292.4.887
- Giannios D., 2013, *MNRAS*, 431, 355. doi:10.1093/mnras/stt167
- Goldreich P., Julian W. H., 1969, *ApJ*, 157, 869. doi:10.1086/150119
- Goodman J., Uzdensky D., 2008, *ApJ*, 688, 555. doi:10.1086/592345
- Haardt F., Maraschi L., 1991, *ApJL*, 380, L51. doi:10.1086/186171
- Hankla A. M., Jiang Y.-F., Armitage P. J., 2020, *ApJ*, 902, 50. doi:10.3847/1538-4357/abb4df
- Hesse M., Cassak P. A., 2020, *JGRA*, 125, e25935. doi:10.1029/2018JA025935
- Hirose S., Krolik J. H., De Villiers J.-P., Hawley J. F., 2004, *ApJ*, 606, 1083. doi:10.1086/383184
- Hoyle F., 1949, *srrs.book*
- Horn B., Lyra W., Mac Low M.-M., Sándor Z., 2012, *ApJ*, 750, 34. doi:10.1088/0004-637X/750/1/34
- Ivanov P. B., Papaloizou J. C. B., Polnarev A. G., 1999, *MNRAS*, 307, 79. doi:10.1046/j.1365-8711.1999.02623.x
- Kanagawa K. D., Tanaka H., Szuszkiewicz E., 2018, *ApJ*, 861, 140. doi:10.3847/1538-4357/aac8d9
- Kelly B. C., Treu T., Malkan M., Pancoast A., Woo J.-H., 2013, *ApJ*, 779, 187. doi:10.1088/0004-637X/779/2/187
- Komissarov S. S., Barkov M. V., 2009, *MNRAS*, 397, 1153. doi:10.1111/j.1365-2966.2009.14831.x
- Krolik J. H., Horne K., Kallman T. R., Malkan M. A., Edelson R. A., Kriss G. A., 1991, *ApJ*, 371, 541. doi:10.1086/169918
- Lee H. K., Wijers R. A. M. J., Brown G. E., 1999, *ASPC*, 190, 173. doi:10.48550/arXiv.astro-ph/9905373
- Li S.-L., Cao X., 2008, *MNRAS*, 387, L41. doi:10.1111/j.1745-3933.2008.00480.x
- Li Y.-P., Chen Y.-X., Lin D. N. C., Zhang X., 2021, *ApJ*, 906, 52. doi:10.3847/1538-4357/abc88310.1002/essoar.10504346.1
- Li X., Guo F., Li H., Li G., 2017, *ApJ*, 843, 21. doi:10.3847/1538-4357/aa745e
- Liang E. P. T., Price R. H., 1977, *ApJ*, 218, 247. doi:10.1086/155677
- Lin D. N. C., Papaloizou J., 1986, *ApJ*, 309, 846. doi:10.1086/164653
- Liu B. F., Mineshige S., Shibata K., 2002, *ApJL*, 572, L173. doi:10.1086/341877
- Liu H., Li S.-L., Guo H., 2016, *MNRAS*, 462, L56. doi:10.1093/mnras/462.1.56
- Liu T., Gu W.-M., Zhang B., 2017, *NewAR*, 79, 1. doi:10.1016/j.newar.2017.07.001
- Loureiro N. F., Schekochihin A. A., Cowley S. C., 2007, *PhPl*, 14, 100703. doi:10.1063/1.2783986
- Lusso E., Risaliti G., 2016, *ApJ*, 819, 154. doi:10.3847/0004-637X/819/2/154
- Lyra W., Paardekooper S.-J., Mac Low M.-M., 2010, *ApJL*, 715, L68. doi:10.1088/2041-8205/715/2/L68
- Lyubarskii Y. E., 1997, *MNRAS*, 292, 679. doi:10.1093/mnras/292.3.679
- Lyubarsky Y., 2009, *ApJ*, 698, 1570. doi:10.1088/0004-637X/698/2/1570
- Manmoto T., Takeuchi M., Mineshige S., Matsumoto R., Negoro H., 1996, *ApJL*, 464, L135. doi:10.1086/310097
- Masset F. S., Papaloizou J. C. B., 2003, *ApJ*, 588, 494. doi:10.1086/373892
- McHardy I. M., 2013, *MNRAS*, 430, L49. doi:10.1093/mnras/430.1.49
- McKernan B., Ford K. E. S., Lyra W., Perets H. B., 2012, *MNRAS*, 425, 460. doi:10.1111/j.1365-2966.2012.21486.x
- McKernan B., Ford K. E. S., Kocsis B., Lyra W., Winter L. M., 2014, *MNRAS*, 441, 900. doi:10.1093/mnras/stu553
- McLaughlin S. A. J., Mullaney J. R., Littlefair S. P., 2024, *MNRAS*, 529, 2877. doi:10.1093/mnras/stae721
- Meusinger H., Henze M., Birkle K., Pietsch W., Williams B., Hatzidimitriou D., Nesci R., et al., 2010, *A&A*, 512, A1. doi:10.1051/0004-6361/200913526
- Narayan R., Igumenshchev I. V., Abramowicz M. A., 2003, *PASJ*, 55, L69. doi:10.1093/pasj/55.6.L69
- Nathanail A., Fromm C. M., Porth O., Olivares H., Younsi Z., Mizuno Y., Rezzolla L., 2020, *MNRAS*, 495, 1549. doi:10.1093/mnras/staa1165
- Paardekooper S., Dong R., Duffell P., Fung J., Masset F. S., Ogilvie G., Tanaka H., 2023, *ASPC*, 534, 685. doi:10.48550/arXiv.2203.09595
- Paardekooper S.-J., Papaloizou J. C. B., 2009, *MNRAS*, 394, 2297. doi:10.1111/j.1365-2966.2009.14512.x
- Paardekooper S.-J., Baruteau C., Crida A., Kley W., 2010, *MNRAS*, 401, 1950. doi:10.1111/j.1365-2966.2009.15782.x
- Parker E. N., 1972, *ApJ*, 174, 499. doi:10.1086/151512
- Parker E. N., 1983, *ApJ*, 264, 642. doi:10.1086/160637
- Pollack J. B., Hubickyj O., Bodenheimer P., Lissauer J. J., Podolak M., Greenzweig Y., 1996, *Icar*, 124, 62. doi:10.1006/icar.1996.0190
- Shakura N. I., Sunyaev R. A., 1973, *A&A*, 24, 337
- Sirko E., Goodman J., 2003, *MNRAS*, 341, 501. doi:10.1046/j.1365-8711.2003.06431.x
- Spitzer L., 1962, *pfig.book*
- Sun M., Xue Y., Brandt W. N., Gu W.-M., Trump J. R., Cai Z., He Z., et al., 2020, *ApJ*, 891, 178. doi:10.3847/1538-4357/ab789e
- Syer D., Clarke C. J., 1995, *MNRAS*, 277, 758. doi:10.1093/mnras/277.3.758
- Tout C. A., Pringle J. E., 1992, *MNRAS*, 259, 604. doi:10.1093/mnras/259.4.604
- Uzdensky D. A., Loureiro N. F., Schekochihin A. A., 2010, *PhRvL*, 105, 235002. doi:10.1103/PhysRevLett.105.235002
- Uzdensky D. A., Goodman J., 2008, *ApJ*, 682, 608. doi:10.1086/588812
- Vaughan S., Edelson R., Warwick R. S., Uttley P., 2003, *MNRAS*, 345, 1271. doi:10.1046/j.1365-2966.2003.07042.x
- Wald R. M., 1974, *PhRvD*, 10, 1680. doi:10.1103/PhysRevD.10.1680
- Wang J.-S., Peng F.-K., Wu K., Dai Z.-G., 2018, *ApJ*, 868, 19. doi:10.3847/1538-4357/aae531
- Ward W. R., 1997, *Icar*, 126, 261. doi:10.1006/icar.1996.5647
- Yuan F., Lin J., Wu K., Ho L. C., 2009, *MNRAS*, 395, 2183. doi:10.1111/j.1365-2966.2009.14673.x
- Yuan F., Wang H., Yang H., 2022, *ApJ*, 924, 124. doi:10.3847/1538-4357/ac4714
- Zenitani S., Hoshino M., 2007, *ApJ*, 670, 702. doi:10.1086/522226
- Zhang B., 2017, *ApJL*, 836, L32. doi:10.3847/2041-8213/aa5ded
- Zhang H., Li X., Guo F., Giannios D., 2018, *ApJL*, 862, L25. doi:10.3847/2041-8213/aad54f
- Zhou S., Sun M., Liu T., Wang J.-M., Wang J.-X., Xue Y., 2024, *ApJL*, 966, L9. doi:10.3847/2041-8213/ad3c3f